### Title

Organizing thermodynamic data obtained from multicomponent polymer electrolytes: Salt-containing polymer blends and block copolymers




### Journal

Journal of Polymer Science Part B Polymer Physics, 57(18)

### ISSN

0887-6266



### Authors

Loo, Whitney S

Balsara, Nitash P



### Publication Date

2019-09-15

### DOI

10.1002/polb.24800

Peer reviewed

# Organizing Thermodynamic Data obtained from Multicomponent Polymer Electrolytes: Salt-Containing Polymer Blends and Block Copolymers

Whitney S. Loo[†], Nitash P. Balsara[†,‡,▯]

[†] Department of Chemical and Biomolecular Engineering, University of California-Berkeley, Berkeley, California 94720, United States

[‡]Materials Sciences Division, Lawrence Berkeley National Laboratory, Berkeley, California 94720, United States

[▯]Joint Center for Energy Storage Research (JCESR), Lawrence Berkeley National Laboratory, Berkeley, California 94720, United States

Correspondence to: Nitash P. Balsara (E-mail: *nbalsara@berkeley.edu*)

**ABSTRACT**

The objective of this review is to organize literature data on the thermodynamic properties of salt-containing polystyrene/poly(ethylene oxide) (PS/PEO) blends and polystyrene-*b*-poly(ethylene oxide) (SEO) diblock copolymers. These systems are of interest due to their potential to serve as electrolytes in all-solid rechargeable lithium batteries. Mean-field theories, developed for pure polymer blends and block copolymers, are used to describe phenomenon seen in salt-containing systems. An effective Flory-Huggins interaction parameter, $\chi_{eff}$, that increases linearly with salt concentration is used to describe the effect of salt addition for both blends and block copolymers. Segregation strength, $\chi_{eff}N$, where $N$ is the chain length of the homopolymers or block copolymers, is used to map phase behavior of salty systems as a function of composition. Domain spacing of salt-containing block copolymers is normalized to account for the effect of copolymer composition using an expression obtained in the weak segregation limit. The phase behavior of salty blends, salty block copolymers, and domain spacings of the latter systems, are presented as a function of chain length, composition and salt concentration on universal plots. While the proposed framework has limitations, the universal plots should serve as a starting point for organizing data from other salt-containing polymer mixtures.

**KEYWORDS**

phase behavior, Flory-Huggins interaction parameter, block copolymers, polymer blends, polymer electrolytes

## AUTHOR BIOGRAPHIES

Whitney S. Loo is currently pursuing her Ph. D. in Chemical and Biomolecular Engineering at University of California, Berkeley. She received her B.S. in Chemical Engineering from MIT in 2015. Her research focuses on synthesizing and characterizing block copolymer electrolytes for applications in next-generation batteries. When she's not in the lab or at the beamline, Whitney practices and teaches yoga.

Nitash P. Balsara is a chemical engineer with a bachelor's degree from the Indian Institute of Technology (IIT) in Kanpur, India, in 1982, a master's degree from Clarkson University in Potsdam, NY, in 1984, a Ph.D. from Rensselaer Polytechnic Institute (RPI) in Troy, NY, in 1988. He did postdoctoral research at the University of Minnesota in Minneapolis, followed by a second postdoc at Exxon Research and Engineering Company in Annandale, NJ. In 1992, he joined the faculty of Department of Chemical Engineering at Polytechnic University in Brooklyn, NY. In 2000, he joined the faculty at the Department of Chemical Engineering at the University of California, Berkeley, and Lawrence Berkeley National Laboratory as a faculty scientist. He has managed to hang on to both jobs. His work on salt-containing polymers is inspired by his colleague and mentor at Berkeley, Professor John Newman.  He cofounded two start-ups, Seeo and Blue Current.

## INTRODUCTION

There is continued theoretical and experimental interest in understanding the thermodynamics and phase behavior of salt-containing polymers due to their applications as solid electrolytes in rechargeable batteries.[1–6] In this review, we consider the effect of added salt on mixtures of two dissimilar homopolymers, A and B, and AB diblock copolymers wherein two dissimilar chains are covalently bonded. The experimentally observed phase behavior of the homopolymer blends and block copolymers is in reasonable agreement with mean-field theory.[7–12] In these theories, phase behavior is determined entirely by two parameters, segregation strength and composition. Segregation strength is characterized by the product $\chi N$, where $\chi$ is the Flory-Huggins interaction parameter and measures the thermodynamic compatibility between A and B chains and $N$ is the degree of polymerization of either the homopolymers or the block copolymer. Composition is quantified by the volume fraction of one of the polymer components, $f_A$. As segregation strength increases (in simple systems this is accomplished by decreasing temperature) polymer blends macrophase separate from a single homogeneous phase into two coexisting phases, one rich in polymer A and another rich in polymer B. The compositions of the coexisting phases depend on both $\chi N$ and $f_A$. As segregation strength increases, block copolymers microphase separate from a homogeneous disordered phase (DIS) into ordered morphologies, such as lamellae (LAM), gyroid phases (GYR), hexagonally packed cylinders (HEX)

and body center cubic spheres (BCC). The geometry of the resulting ordered phase depends on both $\chi N$ and $f_A$.[13–16] The temperature dependence of the Flory-Huggins interaction parameter in salt-free binary polymer systems is generally expressed as

$$\chi = \frac{A}{T} + B \quad (1)$$

where A and B are empirically determined constants.[14,17]

In principle, macrophase separation of homopolymer blends will continue until the denser phase occupies the bottom of the container. In contrast, the periodic length-scale, or domain spacing, obtained in microphase separated systems, $d$, is governed by $\chi N$ and $f_A$.

In this work, we review the literature on the effect of added salt on the thermodynamics of homopolymer blends and block copolymers. Our objective is to organize literature data into a few simple plots. For homopolymer blends, we examine the effect of added salt on the boundary between single-phase and two-phase systems. For block copolymers, we examine the effect of added salt on the phase behavior and domain spacing. Our analysis relies heavily on the mean-field theories discussed above.

## THEORY OF SALT-FREE HOMOPOLYMER BLENDS AND BLOCK COPOLYMERS

The phase diagram of symmetric homopolymer blends is given by the expression[7,17]

$$\chi = \frac{1}{N(1-2f_A)} \ln\left[\frac{1-f_A}{f_A}\right] \quad (2)$$

In Figure 1, we show this phase diagram using $(\chi N)_{norm}$ as the ordinante and $f_A$ as the abscissa. For symmetric homopolymer blends, we define

$$(\chi N)_{norm} = \frac{\chi N}{2} \text{(blends)} \quad (3)$$

because phase separation occurs when $\chi N$ exceeds 2 for a blend with $f_A = 0.5$ .[17] There are no analytical expressions for the boundary between disorder and order for block copolymers. In Figure 1, we show the numerical results for this boundary obtained by Cochran et al. on a $(\chi N)_{norm}$ versus $f_A$ plot.[16] For block copolymers we define

$$(\chi N)_{norm} = \frac{\chi N}{10.495} \text{ (block copolymers)} \quad (4)$$

The normalization constant on the right side of Equation 4 arises because microphase separation occurs when $\chi N$ exceeds 10.495 for a block copolymer with $f_A = 0.5$.[16]

In the weak segregation limit (WSL) *i.e.* in the vicinity of the order-disorder transition (ODT), the composition dependence of the periodic length-scale of ordered block copolymer phases, $d$, was calculated

numerically by Leibler.[9] The length scale of the periodic phase in an ordered block copolymer is a reflection of molecular size. In a homopolymer, molecular size is often characterized by the radius of gyration, $R_g = \frac{N^{\frac{1}{2}} b}{6}$, where $b$ is the statistical segment length of the chain.[7,18] In Leibler's theory, $d$ is given by the product $R_g D$¿) where $D$ is a dimensionless parameter that is a function of the composition of the block copolymer, $f_A$. In Figure 1, we show the results of Leibler on a plot of $D_{norm}$ versus $f_A$. We define

$$D_{norm} = \frac{D}{2.3392} \text{ (periodic length-scale)} \quad (5)$$

The normalization constant on the right side of Equation 4 arises because in Leibler's theory, $D$ is 2.3392 when $f_A$ = 0.5.[9]

The original results described above were fit to simple polynomial expressions

$$(\chi N)_{blends}, (\chi N)_{block\,copolymers} \vee D = C_0 + C_1 (f_A - 0.5)^2 + C_2 (f_A - 0.5)^4 + C_3 (f_A - 0.5)^6 + C_4 (f_A - 0.5)^8 \quad (6)$$

The values for these coefficients for the three curves in Figure 1 are given in Table 1. The $\chi N$ expressions in Equation 6 enable calculation of $\chi$ for homopolymer blends and block copolymers from experimentally observed phase boundaries if $f_A$ and $N$ are known. The $D$ expression in Equation 6

allows for comparisons of $d$ values determined in block copolymers of a given overall chain length with different values of $f_A$.

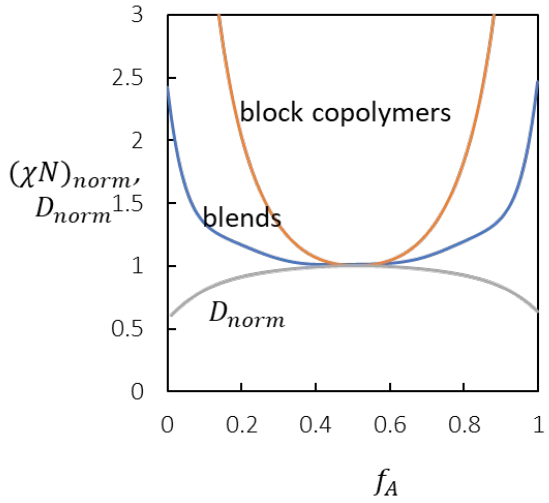


FIGURE 1 Theoretical curves for ¿ for binary polymer blends (blue) and block copolymers (orange) as well as $D_{norm}$ (gray) for block copolymers as a function of composition, $f_A$. See text for definition of these quantities.

TABLE 1 Coefficients for polynomial fits to Equation 6 for the curves given in Figure 1

| | Binary blends | Block copolymers | Periodicity ($D$) |
|---|---|---|---|
| $C_0$ | 2 | 10.495 | 3.2292 |
| $C_1$ | 0.88073 | 47.896 | -2.3226 |
| $C_2$ | 98.693 | 782.17 | -7.6529 |
| $C_3$ | -868.58 | -3566.7 | 33.981 |
| $C_4$ | 2631.4 | 24074 | -211.21 |

## THEORY OF SALT-CONTAINING HOMOPOLYMER BLENDS AND BLOCK COPOLYMERS

The addition of salt to these systems is known to alter their phase behavior due to the introduction of new interactions between the polymers and ions including electrostatic interactions, charge dissociation, ion solvation and physical cross-linking between the ions and polymer chains.

There have been many theoretical studies that attempt to quantify the effects of these interactions on polymer phase behavior. Ions tends to cluster in the phase with the higher dielectric constant and this increases segregation strength. This was captured in models developed by Wang and coworkers using the concept of Born solvation energy.[19,20] In these models, the framework described in the previous section for salt-free systems can be applied to salty systems provided $\chi$ is replaced with an effective interaction parameter, $\chi_{eff}$, which depends on salt concentration. In the simplest case, this dependence is linear and

$$\chi_{eff}=\chi_0+mr \quad (7)$$

where $\chi_0$ is the Flory-Huggins parameter for the salt-free system, $r$ is a suitable measure of salt concentration and $m$ is a system-dependent proportionality constant. This form for $\chi_{eff}$ in salty systems was first proposed in the pioneering work of Mayes and coworkers.[21]

It is important to note that several other theories on the effect of added ions on the thermodynamics of block copolymers and polymer blends have been developed.[22–26] In this study, we use Equation 7 to organize data obtained by different groups on the same plot. The effect of added salt on phase behavior is shown schematically in Figure 2 for both symmetric homopolymer blends and diblock copolymers. As salt concentration increases, miscible blends and copolymers phase separate due to an increase in the effective Flory-Huggins interaction parameter, $\chi_{eff}$.

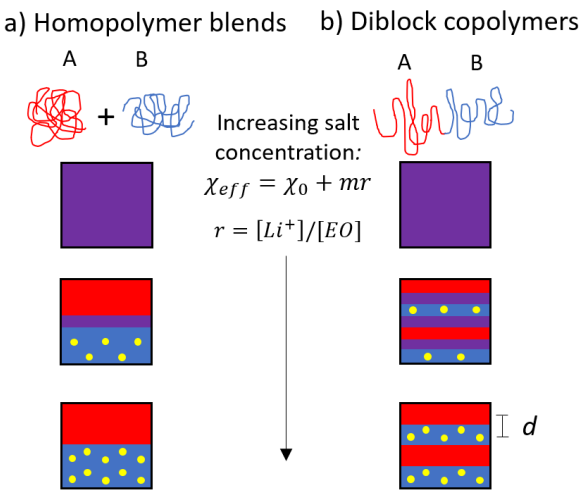


FIGURE 2 Schematic of the effect of increasing segregation due to the addition of salt for symmetric a) homopolymer blends and b) diblock copolymers. As salt concentration, *r*, increases, miscible blends and block copolymers phase separate due to an increase in $\chi_{eff}$. Blends undergo macrophase separation, while block copolymers undergo microphase separation. At low values of $\chi_{eff}$, the interface between the phases is broad, and this broad interface is depicted by a purple band in the schematics. Interfacial thickness becomes negligible at large values of $\chi_{eff}$.

**EXPERIMENTAL SYSTEMS**

The most widely studied systems are blends of polystyrene and poly(ethylene oxide) (PS/PEO) and copolymers of polystyrene-*block*-poly(ethylene oxide) (SEO) mixed with a lithium salt. In this review, we focus on two lithium salts: lithium bis(trifluoromethanesulfonyl)imide (LiTFSI) and lithium trifluoromethanesulfonate (LiTf). These salts maximize the conductivity of PEO-based electrolytes.[27] It is well known that the salt selectively partitions into the PEO domain due to specific interactions between ether oxygens and $Li^+$ ions and the relatively high dielectric constant of PEO.[28–30] Table 2 shows the molecular weights, chain lengths and compositions of the materials considered in this study as well as the salt

species used for the electrolytes, taken from refs 31–38. Included in this list are a PEO homopolymer, a PS homopolymer and 22 SEO block copolymers. Both homopolymers and copolymers are named according to their molecular weights. For example, S(0.6) refers to a polystyrene homopolymer with $M_{PS}$ = 0.6 kg mol$^{-1}$ and SEO(1.9-0.8) refers to a SEO copolymer with $M_{PS}$ = 1.9 kg mol$^{-1}$ and $M_{PEO}$ = 0.8 kg mol$^{-1}$.

TABLE 2 Characteristics of polymers used in this study

| Polymer | $M_{PS}$ (kg mol$^{-1}$) | $M_{PEO}$ (kg mol$^{-1}$) | $f_{EO}$ | $N$ | Salt Species | *Ref* |
|---|---|---|---|---|---|---|
| **EO(0.55)** | 0 | 0.55 | - | 8.7 | LiTFSI | Xie[31] |
| **S(0.6)** | 0.6 | 0 | - | 10 | LiTFSI | Xie[31] |
| **SEO(1.9-0.8)** | 1.9 | 0.8 | 0.29 | 42 | LiTFSI | Teran[32] |
| **SEO(1.4-1.6)** | 1.4 | 1.6 | 0.52 | 46 | LiTFSI | Teran[32] |
| **SEO(1.7-1.4)** | 1.7 | 1.4 | 0.44 | 48 | LiTFSI | Teran[32] |
| **SEO(2.9-3.3)** | 2.9 | 3.3 | 0.52 | 94 | LiTFSI | Teran[32] |
| **SEO(2.3-4.6)** | 2.3 | 4.6 | 0.65 | 104 | LiTFSI | Wanakule[33] |
| **SEO(3.1-5.1)** | 3.1 | 5.1 | 0.60 | 124 | LiTFSI | Wanakule[33] |
| **SEO(4.6-3.7)** | 4.6 | 3.7 | 0.43 | 127 | LiTFSI | Wanakule[33] |
| **SEO(5.3-3.0)** | 5.3 | 3.0 | 0.35 | 128 | LiTFSI | Wanakule[33] |
| **SEO(5.3-3.6)** | 5.3 | 3.6 | 0.39 | 137 | LiTFSI | Wanakule[33] |
| **SEO(4.9-5.5)** | 4.9 | 5.5 | 0.52 | 158 | LiTFSI | Teran[32] |
| **SEO(3.8-8.2)** | 3.8 | 8.2 | 0.68 | 180 | LiTFSI | Loo[34] |
| **SEO(9.4-2.4)** | 9.4 | 2.4 | 0.20 | 184 | LiTFSI | Loo[34,38] |
| **SEO(6.4-7.2)** | 6.4 | 7.2 | 0.51 | 207 | LiTFSI | Teran[32] |

| | | | | | | |
|---|---|---|---|---|---|---|
| **SEO(9.4-4.0)** | 9.4 | 4.0 | 0.29 | 208 | LiTFSI | Loo[34,38] |
| **SEO(6.4-7.3)** | 6.4 | 7.3 | 0.52 | 210 | LiTFSI | Teran[32] |
| **SEO(10.0-4.5)** | 10 | 4.5 | 0.30 | 224 | LiTf | Young[36] |
| **SEO(9.5-8.0)** | 9.5 | 8.0 | 0.44 | 268 | LiTf | Gunkel[35] |
| **SEO(5.1-12.8)** | 5.1 | 12.8 | 0.72 | 269 | LiTFSI | Loo[34] |
| **SEO(9.7-10.4)** | 9.7 | 10.4 | 0.50 | 307 | LiTf | Zardalidis[37] |
| **SEO(17.4-3.9)** | 17.4 | 3.9 | 0.18 | 333 | LiTFSI | Loo[34,38] |
| **SEO(4.0-22.4)** | 4.0 | 22.4 | 0.85 | 393 | LiTFSI | Loo[34] |
| **SEO(48.6-41.4)** | 48.6 | 41.4 | 0.44 | 1379 | LiTf | Zardalidis[37] |

Chain length, $N$, was calculated by $N = N_{PS} + N_{PEO}$ where

$$N_i = \frac{M_i}{\rho_i N_A \nu_{ref}} \quad (i = \text{PS or PEO}) \quad (8)$$

$N_A$ is Avogadro's number and $\nu_{ref}$ was fixed at 0.1 nm$^3$. The volume fractions of each block of the copolymers were calculated by

$$f_{EO} = \frac{\nu_{EO}}{\nu_{EO} + \frac{M_{PS} M_{EO}}{M_S M_{PEO}} \nu_S} \quad (9)$$

where $\nu_{EO}$ and $\nu_S$ are the molar volumes of ethylene oxide and styrene monomer units, respectively, and $M_{EO}$ and $M_S$ are the molar masses of ethylene oxide (44.05 g mol$^{-1}$) and styrene (104.15 g mol$^{-1}$), respectively. $M_{PS}$ and $M_{PEO}$ are the number averaged molecular weights of the PS and PEO blocks in kg mol$^{-1}$ provided in Table 1. Molar volumes were calculated by

$\nu = M/\rho$. In this study, the densities (g $cm^{-3}$) of the PEO and PS blocks were given by $\rho_{PEO}=1.13$ and $\rho_{PS}=1.05$, measured values at 90 °C.

For the salty samples, we assume that all of the salt resides in the PEO domain.[29,30] Both homopolymer blends and block copolymers containing salt are considered to be pseudo-binary systems where the volume fraction of the salt + PEO component is given by

$$f_{EO,salt}=\frac{\nu_{EO,LiTFSI}(r)}{\nu_{EO,LiTFSI}(r)+\left(\frac{M_{PS}M_{EO}}{M_S M_{PEO}}\nu_S\right)} \quad (10)$$

where $r$ is the molar ratio of $Li^+$ to ethylene oxide (EO) moieties ($r=$¿¿) and $\nu_{EO,LiTFSI}$ is the molar volume of the salt-containing PEO phase calculated by

$$\nu_{EO,LiTFSI}(r)=\frac{M_{EO}}{\rho_{EO,LiTFSI}(r)} \quad (11)$$

where

$$\rho_{EO,LiTFSI}(r)=2.008r+1.13 \quad (12)$$

taken from ref 39. Because the effect of LiTf on the density of PEO has not been measured, ideal mixing was assumed such that

$$f_{EO,salt}=\frac{\nu_{EO}+r\,\nu_{LiTf}}{\nu_{EO}+r\,\nu_{LiTf}+\left(\frac{M_{PS}M_{EO}}{M_S M_{PEO}}\nu_S\right)} \quad (13)$$

where $v_{LiTf}=\frac{M_{LiTF}}{\rho_{LiTf}}$ , $\rho_{LiTf}$=1.90 g cm$^{-3}$ and $M_{LiTf}$=155.95 g mol$^{-1}$.

**FLORY-HUGGINS INTERACTION PARAMETER, $\chi$**

We begin with a discussion on cloud point measurements of a polymer blend of PS ($M$ = 0.55 kg mol$^{-1}$, $N$ = 8.7) and PEO ($M$ = 0.6 kg mol$^{-1}$, $N$ = 10) (S(0.6)/EO(0.55)) mixed with LiTFSI reported by Xie et al.[31] The cloud point temperatures ($T_{cp}$) depends on the PS/PEO ratio in the blends and $r$. This data set is presented in Figure 3a where the phase boundary between one-phase and two-phase systems is shown on a plot of $f_{EO,salt}$ versus $r$ at different temperatures. Equation 10 was used to calculate $f_{EO,salt}$ from the raw data in ref 31. For each salt concentration, $0.01 \le r \le 0.06$, compositions of the PEO-rich phase were determined at cloud point temperatures of 80, 100, 120, and 150 ° C. Both $T_{cp}$ and $f_{EO,salt}$ increase with salt concentration. Equation 6, which relates segregation strength and composition at the phase boundary of binary blends, was used to determine $\chi_{eff}$ at a given temperature from the data in Figure 3a. For a given salty PS/PEO blend, the value of $\chi_{eff}$ at the cloud point, was calculated according to

$$\chi_{eff}=\frac{C_0+C_1\left(f_{EO,salt}-0.5\right)^2+C_2\left(f_{EO,salt}-0.5\right)^4+C_3\left(f_{EO,salt}-0.5\right)^6+C_4\left(f_{EO,salt}-0.5\right)^8}{N} \quad (14)$$

where coefficients, $C_i$'s, for the case of blends are used (see Table 1). Equation 14 is obtained from Equation 6 with the with the assumption that $f_A=f_{EO,salt}$. Here, $N$ was taken to be 9.35, the average of $N_{PS}$ and $N_{PEO}$.

Equation 14 allows for the determination of values of $\chi_{eff}$ for a given polymer blend at a specific temperature and value of $f_{EO,salt}$. The results of these calculations are plotted as solid data points in Figure 3b as a function of *r,* at the temperatures specified in Figure 3.

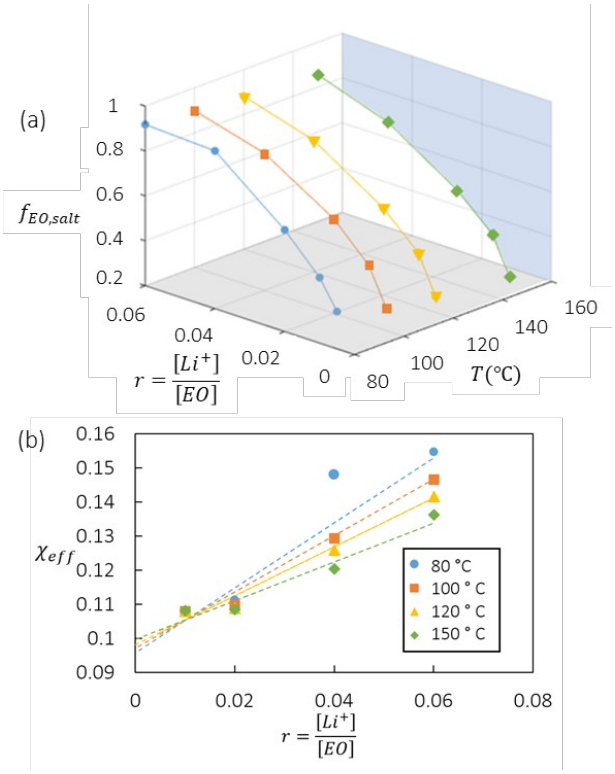


FIGURE 3 a) Phase boundary between single-phase and two-phase systems in salty S(0.6)/ EO(0.55) blends shown on a plot of blend composition $f_{EO,salt}$, as a function of salt concentration, *r*, and temperature, *T*, taken from ref 31. Data is shown for T = 80 (blue circles), 100 (orange squares), 120 (yellow triangles) and 150 °C (green diamonds). A projection to the two-phase region is shown in blue. b) Effective Flory-Huggins interaction parameter, $\chi_{eff}$ , for PS/PEO blends as a function of salt concentration, *r*, at temperatures as indicated. Data points are experimental values and dashed lines show a fit through Equation 15.

Building on the functional form of $\chi$ for salt-free systems, provided in Equation 1, we propose the following extension for salty systems:

$$\chi_{eff}=\frac{(Ar+B)}{T}+Cr+D \quad (15)$$

The lines in Figure 3b are least squares fits of Equation 15 through the data which give $A=818.41$ ($K^{-1}$), $B=-8.2332$ ($K^{-1}$), $C=-1.3625$ and $D=0.1109$. Because the neat polymer blends were miscible at all temperatures, values for $\chi_0$ could not be determined explicitly. However, $\chi_0$ can be calculated by setting $r=0$ in Equation 15. In this work we focus on data at 100 °C where $\chi_0=0.097$, which is in agreement with previously reported literature values.[40]

Next, we determined $\chi_{eff}$ values for SEO block copolymer electrolytes as a function of salt concentration. Our approach is similar to that described above for polymer blends. The boundary between disordered and microphase separated salty SEO copolymers with different values of $f_{EO,salt}$ and $N$ was determined experimentally. Equation 6 with $C_i$'s corresponding to the case of block copolymers (see Table 1) was then used to determine $\chi_{eff}$ at the phase boundary. Gunkel et al.[35] and Wanakule et al.[33] mapped the phase boundary in a set of salt-containing SEO copolymers, and the order-disorder transition temperatures ($T_{ODT}$) obtained ranged from 95 – 240 °C shown in Figure 4 (blue squares). Loo et al.[34] used the same approach but their data were obtained at a fixed temperature of 100 °C. These data are also shown in Figure 4 (yellow circles). The dashed line in Figure 4 represents an expression for $\chi_{eff}$ reported in ref 34:

$$\chi_{eff} = \chi_0 + 1.66\, r \quad (16)$$

where $\chi_0$ appropriate for neat block copolymers is 0.047.[41] In principle, $\chi_0$ for blends and block copolymers should be identical. However, many studies have shown that the numerical values of $\chi$ obtained in blends and block copolymers can differ substantially.[40,42–44] Based on temperature-dependent chi parameter for symmetric SEO/LiTFSI mixtures given in ref 32, we expect $\chi_{eff}$ to change by less than 10% in the temperature window between 95 -240 °C. Thus, $\chi_{eff}$ is a much stronger function of salt concentration, changing by over 200% over the salt concentration range of interest. We thus plot $\chi_{eff}$ reported by Gunkel et al.[35], Wanakule et al.[33], and Loo et al.[34] on the same plot (Figure 4), ignoring the differences in temperature used in these studies.

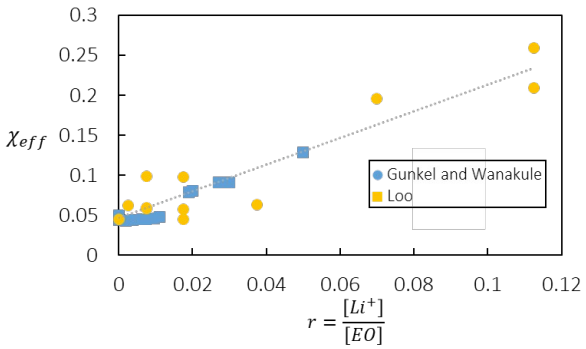


FIGURE 4 Salt concentration dependence of $\chi_{eff}$ for block copolymers when mapped to mean-field theory at an order-disorder transition for Gunkel and Wanakule (blue squares) as well as for Loo (yellow circles). The dashed line represents a least-squares linear regression fit through both data sets according to Equation 16.

## PHASE BEHAVIOR

We begin by discussing the phase behavior of salt-containing PS/PEO blends at 100 °C. The boundary between single-phase and two-phase systems is plotted on a universal $\chi_{eff}N$ versus $f_{EO,salt}$ plot in Figure 5 using Equation 6 (with $C_i$'s corresponding to polymer blends). The shaded blue region represents the two-phase region calculated and the white region represents the homogeneous single-phase region taken from ref 17. The dependence of segregation strength ($\chi_{eff}N$) for salty S(0.6)/ EO(0.55) at 100 °C can readily be calculated by multiplying both sides of Equation 15 by $N$:

$$\chi_{eff}N = 0.83rN + 0.097N \quad (17)$$

The data points correspond to the 100 °C data shown in Figure 3b, and Equation 17 was used to calculate $\chi_{eff}N$ as a function of salt concentration, $r$. The agreement between theory and experiment is reasonable. In principle, Figure 5 in conjunction with Equation 17 should apply to all salt-containing PS/PEO blends regardless of chain length. Nevertheless, Figure 5, and the methodology presented here to place data on it, should serve as a starting point for organizing the phase behavior of other salt-containing polymer blends when such data becomes available.

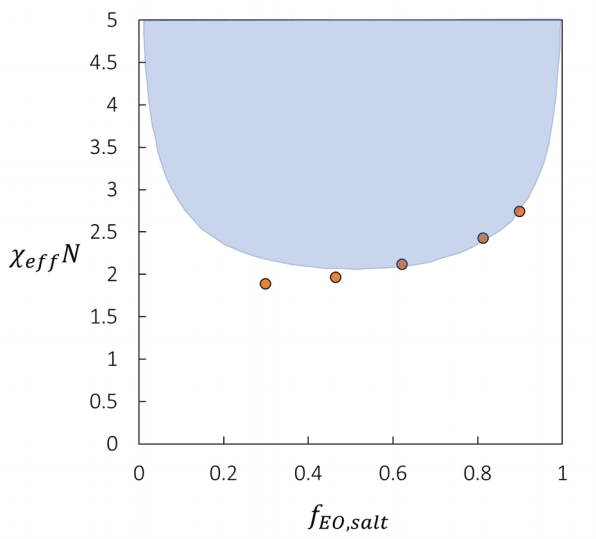


FIGURE 5 Phase diagram for salt-containing PS/PEO homopolymer blends taken at 100 °C plotted as $\chi_{eff}N$ versus $f_{EO,salt}$. The shaded regions represent phase boundaries calculated by mean-field SCFT for salt-free systems and the data points are discrete samples. Data from only one blend system is currently in the literature (see Table 2).

We now discuss the phase behavior of salt-containing SEO block copolymers at 100 °C. The boundary between single-phase and microphase separated systems is plotted on a universal $\chi_{eff}N$ versus $f_{EO,salt}$ plot in Figure 6 using Equation 6 (with $C_i$'s corresponding to block copolymers). The phase boundaries for ordered morphologies within the microphase separated region, replicated from ref 16, represent results from SCFT calculations for neat block copolymers. BCC is shown in orange, HEX in green, GYR in blue and LAM in pink. Multiplying both sides of Equation 16 by $N$, we get the dependence of segregation strength on salt concentration for salt-containing SEO copolymers at 100 °C:

$$\chi_{eff}N = 0.047N + 1.67Nr \quad (18)$$

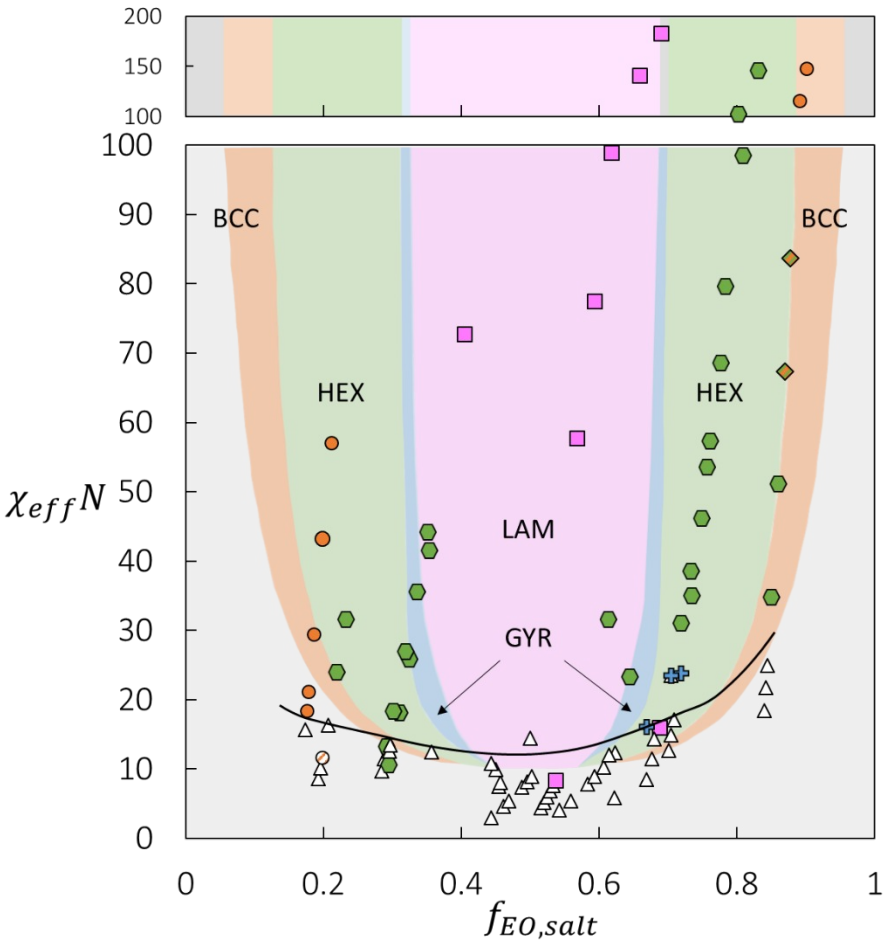


FIGURE 6 Phase diagram for salt-containing SEO block copolymers blends taken at 100 °C plotted as $\chi_{eff}N$ versus $f_{EO,salt}$. The shapes of the symbols correspond to the morphologies of the electrolytes: Δ for DIS (white), ○ for BCC (orange), □ for LAM (pink), ⎔ for HEX (green), and +¿ for GYR (blue). The shaded regions represent phase boundaries calculated by mean-field SCFT for salt-free systems and the data points are discrete samples.

The discrete data points in Figure 6 represent morphologies determined by small angle X-ray scattering (SAXS) experiments for a given SEO electrolyte, characterized by $N$, $f_{EO,salt}$ and $r$. $\chi_{eff}N$ for a given SEO electrolyte is then calculated by Equation 18. The symbols for each electrolyte correspond to their morphology: BCC is given as circles, HEX as hexagons, GYR as plus signs, LAM as squares, and DIS as triangles. Due to

the sparseness of data at $\chi_{eff}N > 100$, the figure is broken up into two panels. We assume that the phase boundaries are vertical when $\chi_{eff}N$>100 in accordance with strong segregation theory.[16,45,46]

Overall, there is agreement between SCFT calculations and the experimental data. The experimentally determined location of the order-disorder boundary is shown by a black curve in Figure 6. It was determined by locating the order-disorder transition at $f_{EO,salt}$=0.18, 0.29, 0.72, and 0.86 and joining these data points by lines. A large majority of the open triangles (but not all of them), corresponding to the DIS phase, in Figure 6 are located below the order-disorder curve. Similarly, there are a few ordered phases that fall below the experimental order-disorder curve; these samples are typically the highest salt concentration of a given low molecular weight SEO. The agreement is perhaps surprising given the simplicity of Equation 18. At low $f_{EO,salt}$ values (in the vicinity of 0.2), the experimental boundary between BCC and HEX occurs at slightly higher $f_{EO,salt}$ values than those predicted by theory. At 0.3<$f_{EO,salt}$<0.4, the experimentally determined boundary between HEX and LAM also occurs at slightly higher $f_{EO,salt}$ values than those predicted by theory. In symmetric systems near $f_{EO,salt}$=0.5, LAM is obtained as predicted by theory, especially when $\chi_{eff}N$>50. As $f_{EO,salt}$ values approach 0.6, we obtained HEX experimentally, but theory predicts LAM. On the PEO-rich side of the phase diagram, there is excellent agreement between experimentally determined HEX phases and theoretical predictions between

0.7<$f_{EO,salt}$<0.8. The data points that are filled with hatched patterns represent samples that exhibited coexistence between two ordered morphologies.[34,38] The phase boundary between HEX and BCC at values of $\chi_{eff}N$>60 on the $f_{EO,salt}$>0.5 side aligns extremely well with experiment. Pure BCC phases are seen in this region at $\chi_{eff}N$>100, as predicted by theory.

**DOMAIN SPACING**

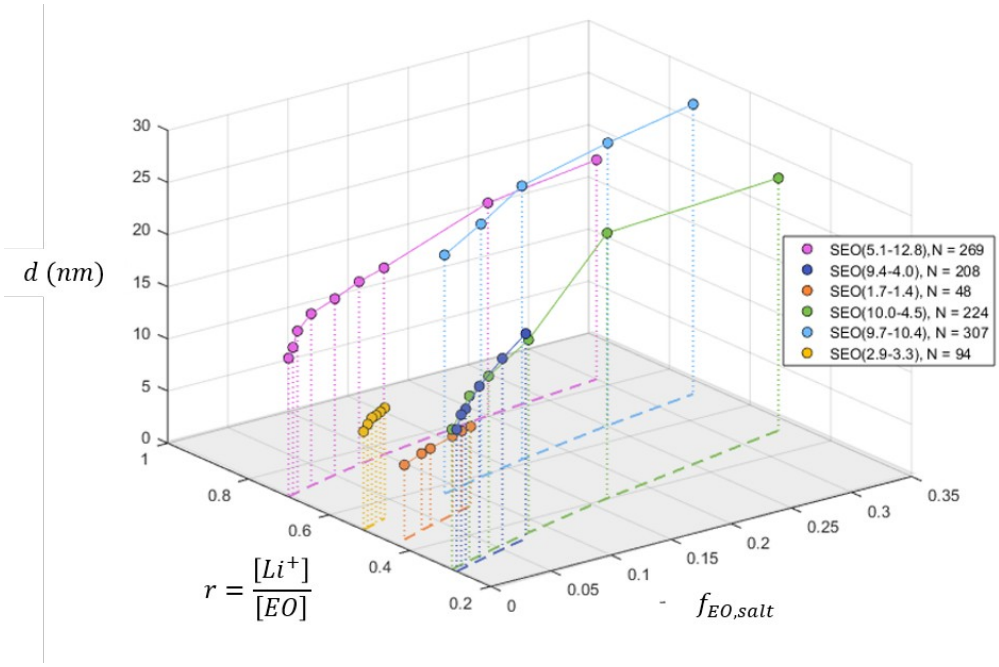


FIGURE 7 3D plot of volume fraction of PEO + salt, $f_{EO,salt}$, domain spacing, $d$, and salt concentration, $r$, for a sample of SEO copolymers used in this study at 120 °C. Dashed lines shown are a projection to the $d$=0 plane.

We conclude with a discussion on the effect of salt on the domain spacing of the SEO copolymers. Figure 7 shows selected data from a subset of SEO copolymers included in Table 2. Domain spacing, $d$, is plotted as a function of volume fraction of the salt containing phase, $f_{EO,salt}$, and salt

concentration, $r$, at 120 °C. The values of $N$ are given in the legend. It is obvious from Figure 6 that the relationship between $d$, $N$, $r$, and $f_{EO,salt}$ is complicated. It is evident in Figure 6 that $f_{EO,salt}$ increases monotonically as $r$ increases; see the dashed curves in the bottom $f_{EO,salt}$–$r$ plane (i.e. $d$=0 plane) in the figure. The dashed curves in Figure 6, which are based on Equations 10-12, are slightly non-linear. It is also evident in Figure 6 that $d$ increases with increasing $r$ but the relationship between these variables is highly non-linear. It is thus helpful to account for the dependence of d on the two relevant variables ($f_{EO,salt}$ $r$) independently.

To account for the dependence of $d$ on $f_{EO,salt}$, we normalize $d$ by $D$ defined in the Introduction (see Equation 6 with $C_i$'s corresponding to periodicity from Table 1). Figure 8 is a plot of normalized domain spacing ( $D=\frac{d}{D}$) versus salt concentration, $r$, at 120 °C. (We chose 120 °C because of the availability of published data. The plot would be much sparser if we used available data at 100 °C, the temperature used in the discussion of phase behavior. We do not expect qualitative differences due to this 20 °C discrepancy in temperature.) The data in Figure 8 are color coded with the same color scheme used to describe the morphologies of SEO block copolymers in Figure 6. The symbols for the discrete data points correspond to the morphology of a given electrolyte; they also match the symbols used in Figure 6. On this plot, the disordered systems (DIS) appear towards the

lower half, and in this regime, $D$ is more-or-less independent of $r$. In disordered systems, the reported value of $d$ corresponds to the characteristic length scale of concentration fluctuations.[9] In the ordered state, $D$ increases with $r$ in a non-linear fashion, increasing more rapidly at higher values of $r$. When coexistence of ordered phases was observed for a single electrolyte, domain spacing for each morphology is presented. It is worth noting that in Figure 8, different morphologies are segregated into different pockets on the $D$ versus $r$ plot. The LAM pocket occurs at the upper right-hand corner of the diagram, GYR and HEX phases appear in the middle of the diagram above DIS but below BCC. Interestingly, the BCC pocket runs into the LAM pocket in the vicinity of $r=0.1$. There are two outliers of LAM seen inside the DIS region. In these two electrolytes, the DIS phase was transformed into LAM by the addition of salt. In contrast, the LAM phases presented in the upper right-hand corner of Figure 8 were obtained in electrolytes with inaccessible order-disorder transitions.

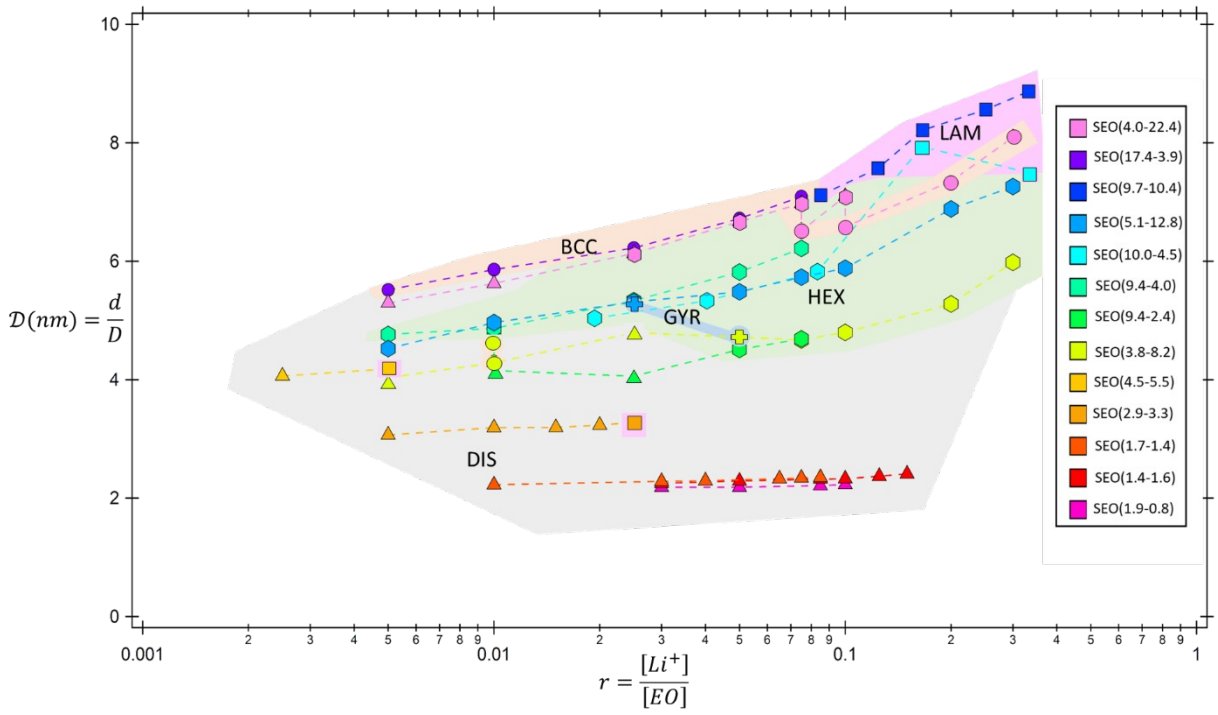


FIGURE 8 Dependence of normalized domain spacing, $D = \frac{d}{D}$, on salt concentration, $r$, for salt-containing SEO block copolymers at 120 °C. Data from different morphologies cluster into "pockets" that are colored differently and match Figure 6: DIS (gray), BCC (orange), LAM (pink), HEX (green), and GYR (blue). The symbols indicate the morphology and also match those of Figure 6: Δ for DIS, ○ for BCC, □ for LAM, ⎔ for HEX, and +¿ for GYR. Dashed lines are a guide for the eye.

If the change in domain spacing upon salt addition was only due to changes in $f_{EO,salt}$, then within our framework, $D$ would be independent of salt concentration for each polymer as our normalization scheme (Equation 6) accounts for this effect. It is, however, clear from Figure 8 that the changes in domain spacing upon salt addition are due to additional effects introduced by the presence of ions such as increased segregation. In each of the ordered morphologies, the junction between PS and PEO chains are located near the domain boundaries. Segregation strength is known to affect

the area per junction.[47,48] It is evident that the addition of salt to ordered morphologies results in a decrease in the area per junction.

Figure 9 shows the relationship between normalized domain spacing, $D$, chain length, $N$, and segregation strength, $\chi_{eff}N$, for the SEO copolymers with and without salt. The ordinate in Figure 9 is a dimensionless quantity: $\frac{D}{bN^{\frac{1}{2}}}$; note that $D$ has units of nm. The statistical segment length, $b$, was taken to be 0.5 nm, the nominal value that applies to a large number of flexible polymer chains.[49] (Although it is likely that the presence of salt affects the statistical segment length of PEO, no quantitative data exists for the relationship between $b$ and $r$.[28] We therefore, hold $b$ constant at 0.5 nm for all salt concentrations as a first approximation.) All of the data in Figure 8 collapses on to two straight lines in Figure 9. The solid lines are vertically shifted linear regressions through the dataset cut off at $\chi_{eff}N \leq 10$.. The break in the data at $\chi_{eff}N=10$ is expected as the systems cross-over from the weak to strong segregation limit.

Based on the $\chi_{eff}N \leq 10$ data set, we obtain

$$\frac{D}{bN^{\frac{1}{2}}}=0.63 \quad (19)$$

Based on the $\chi_{eff}N>10$ data set, we obtain

$$\frac{D}{bN^{\frac{1}{2}}}=0.42\left(\chi_{eff}N\right)^{0.177} \quad (20)$$

The constants in each regression were modified slightly to enforce continuity at $\chi_{eff}N=10$ (from 0.656 to 0.63 in Equation 19 and from 0.404 to 0.420 in Equation 20). The dashed lines around each line represent 95% confidence intervals for the modified regressions. At low values of segregation strength, $\chi_{eff}N \ll 10$, the right side of Equation 20 is independent of $\chi_{eff}N$ and $D \sim N^{\frac{1}{2}}$ as predicted by the mean field theory of Leibler.[9] At high values of segregation strength where ordered phases are obtained, $\chi_{eff}N \gg 10$, $D \sim N^{\frac{2}{3}}$ as predicted in the strong segregation limit (SSL).[45,46,50] The observed crossover in Figure 9 from weak to strong segregation is consistent with the theory of Uneyama and Doi wherein a monotonic increase in the $D$ versus $N$ exponent is predicted at the crossover.[51] The theory of Matsen and Bates predicts a higher exponent for the $D$ versus $N$ scaling at intermediate segregation strength $\left(10<\chi_{eff}N<100\right)$.[46] The data in Figure 9 do not agree with this prediction. It is worth noting that neither theory was developed for salt-containing block copolymers.

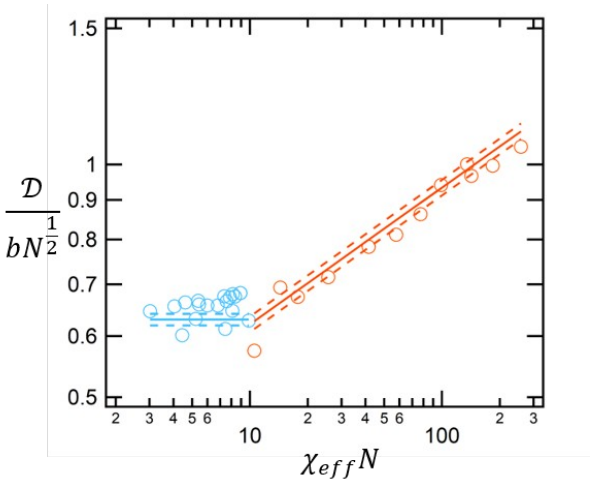


FIGURE 9 Relationship between normalized domain spacing, chain length, and segregation strength for the salt-containing SEO copolymers. In the WSL, $\chi_{eff}N>10$, the normalized domain spacing is independent of segregation strength. In the SSL, $\chi_{eff}N>10$, $D \sim N^{\frac{2}{3}}$. Experimental data in the weak and strong segregation regimes are shown in blue and orange circles, respectively. The solid lines represent Equations 19 and 20, based on linear regressions as described in the text. The dashed lines represent a 95% confidence interval for the two data sets.

In the vicinity of the disordered regime, where $\chi_{eff}N \leq 10$, we can re-arrange Equation 19 to give

$$\frac{d}{D} = 0.315 N^{\frac{1}{2}} \qquad \text{for } \chi_{eff}N<10 \quad (21)$$

Note, in this limit, normalized domain spacing is independent of $\chi_{eff}$.

In the ordered regime, where $\chi_{eff}N>10$, we substitute Equation 18 into Equation 20 and arrive at an explicit expression for the dependence of $d$ on $f_{EO,salt}$, $N$, and $r$:

$$\frac{d}{D}=0.21\,N^{0.667}\left(0.047+1.67\,r\right)^{0.177} \text{ for } \chi_{eff}N\geq 10 \quad (22)$$

Note, the right sides of Equations 21 and 22 are equal at $\chi_{eff}N=10$.

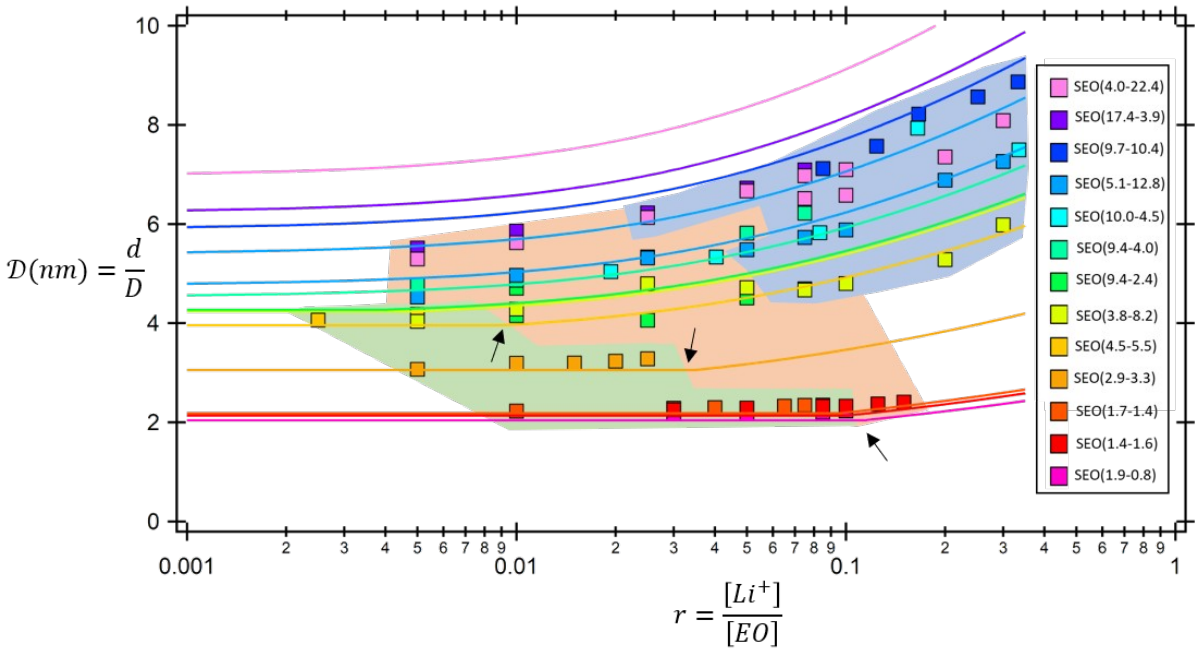


FIGURE 10 Comparison of predictions and experiment for normalized domain spacing, $D$, as a function of salt concentration, $r$, according to Equations 21 (WSL) and 22 (SSL). The squares show data corresponding to the system indicated in the legend. Curves of the same color indicate theoretical predictions for individual systems. The legend is organized according to the relative magnitude of fancy D. For example, the topmost curve corresponds to SEO(4.0-22.4), the top entry in the legend. The shaded regions represent different regimes of segregation strength: $\chi_{eff}N<10$ (green), $10\leq\chi_{eff}N<30$ (orange), and $\chi_{eff}N\geq 30$ (blue). The three black arrows denote the cross-over from Equations 21 to 22 at $\chi_{eff}N=10$ for the low molecular weight SEO copolymers (N < 158). For cases with N > 158, only Equation 22 is used; the cross-over is predicted to occur at $r$ that is below 0.001.

Equations 21 and 22 provide explicit predictions of domain spacing as a function of $N$, $r$, and $f_{EO,salt}$. It is instructive to re-examine the data in Figure

8 in light of these expressions. The data in Figure 8 are replotted in Figure 10. The solid lines in Figure 10 represent Equations 21 and 22. There are three shaded regions that represent different regimes of segregation strength: $\chi_{eff}N<10$ (green), $10\leq\chi_{eff}N<30$ (orange), and $\chi_{eff}N\geq30$ (blue). Note, only five SEO copolymers, which lie at the bottom of Figure 10, are within the weak segregation limit with $N<158$ (green region); we see good agreement between these data and Equation 21. There are three black arrows in Figure 10; they show the transition between Equations 21 and 22 for the low molecular weight SEO copolymers. The remaining SEO copolymers are long enough to have $\chi_{eff}N>10$ for all studied salt concentrations (orange and blue regions). We see good agreement between experiment data and Equation 22 for some of the systems with $10\leq\chi_{eff}N<30$ (orange region). At higher segregation strengths (blue region), the predicted increase in $D$ with $r$ is much stronger than that observed experimentally. These deviations are not evident when the data is presented on a log-log plot (Figure 9). There are thus some unresolved issues that arise in the strongly segregated salty block copolymers.

A possible explanation for the discrepancy between theory and experiments seen in Figure 10 is the limited applicability of our expression for $\chi_{eff}N$ (Equation 18). The linear relationship between $\chi_{eff}$ and $r$ presented in that equation is likely to be valid over a limited range of salt concentrations. This discrepancy has been seen experimentally in salt-

containing symmetric SEO copolymers with $f_{EO,salt}$ values in the vicinity of 0.5. Over the limited range of $r$ and $N$ values covered in ref 32, the dependence of $\chi_{eff}$ on these parameters was given by

$$\chi_{eff} = A + \frac{B}{N} + \frac{C}{N}\left[1 - \exp\left(\frac{-Dr}{N}\right)\right] \quad (23)$$

This expression suggests that $\chi_{eff}$ does not increase linearly over an indefinite range of salt concentrations; at concentrations above a certain threshold (e.g. $r = 0.012$ at $N = 100$), $\chi_{eff}$ levels off. Based on our analysis thus far, we can assert that this expression does not apply over the range of compositions covered in this review. One may thus view Equations 21 and 22 as a starting point for organizing domain spacing data from salt-containing block copolymers.

**CONCLUSIONS**

The objective of this review is to organize literature data on the thermodynamic properties of PS/PEO blends and SEO diblock copolymers with added salt. Our organization strategy relies heavily on theories developed for pure block copolymers and blends. While data from several SEO copolymers are in the literature, data from only one PS/PEO blend has been published. A more systematic study of polymer electrolyte blends seems warranted.

The effect of added salt is captured by defining an effective Flory-Huggins interaction parameter, $\chi_{eff}$, that increases linearly with salt

concentration, $r$. Slightly different linear expressions were developed for blends and block copolymers (Equations 15 and 16). These expressions for $\chi_{eff}$ enable mapping of the phase behavior of both systems on to universal phase diagrams (Figures 5 and 6) developed for salt-free systems. The dependence of domain spacing, $d$, on $N$, $r$, and $f_{EO,salt}$ for SEO block copolymers collapses on to two universal lines for weak and strong segregation, respectively. This collapse was only obtained after $d$ was normalized by a function that we call $D(f_{EO,salt})$ that was first introduced by Leibler. The dimensionless domain spacing, $D/(bN^{\frac{1}{2}})$ is a constant in the weak segregation limit and scales with $\chi_{eff}N$ in the strong segregation limit. The same expression for $\chi_{eff}N$ is used to organize both phase behavior and domain spacing data of salty block copolymers. It is likely, however, that the dependence of $\chi_{eff}$ on salt concentration deviates from linearity at high salt concentrations. We hope that this effect will be addressed by the community in future studies.

**ACKNOWLEDGEMENTS**

Primary funding for this work was provided by the National Science Foundation through Award DMR-1505444. W.S.L. acknowledges funding from the National Science Foundation Graduate Student Research Fellowship DGE-1106400.

**LIST OF SYMBOLS**

| | |
|---|---|
| $b$ | statistical segment length (nm) |
| $d$ | domain spacing (nm) |
| $D$ | Periodicity |

| | |
|---|---|
| $D_{norm}$ | normalized periodicity |
| $D$ | normalized domain spacing (nm) |
| $f_A$ | volume fraction of species A |
| $M_i$ | number-averaged molecular weight of species i (kg $mol^{-1}$) |
| $N$ | number-averaged degree of polymerization (sites $chain^{-1}$) |
| $r$ | salt concentration ($[Li^+]$ $[EO]^{-1}$) |
| $R_g$ | radius of gyration (nm) |

Greek

| | |
|---|---|
| $\chi$ | Flory-Huggins interaction parameter |
| $\chi_0$ | Flory-Huggins interaction parameter of salt free system |
| $\chi_{eff}$ | effective Flory-Huggins interaction parameter |
| $\chi N$ | segregation strength |
| $(\chi N)_{norm}$ | normalized segregation strength |
| $\nu_i$ | molar volume of species i ($cm^3$ $mol^{-1}$) |
| $\nu_{ref}$ | reference volume ($nm^3$ $site^{-1}$) |
| $\rho_i$ | density of species i (g $cm^{-3}$) |

**LIST OFABBREVIATIONS**

| | |
|---|---|
| BCC | body center cubic |
| DIS | disordered |
| EO | ethylene oxide |
| GYR | gyroid |
| HEX | hexagonally packed cylinders |
| LAM | lamellar |
| LiTf | lithium trifluoromethanesulfonate salt |
| LiTFSI | lithium bis(trifluoromethanesulfonyl) imide salt |
| $N_A$ | Avogadro's number |
| ODT | order-disorder transition |
| PEO | poly(ethylene oxide) |
| PS | polystyrene |
| S | styrene |
| SAXS | small angle X-ray scattering |
| SCFT | Self Consistent Field Theory |
| SEO | polystyrene-*block*-poly(ethylene oxide) |
| SSL | strong segregation limit |
| $T_{cp}$ | cloud point temperature (°C) |

| | |
|---|---|
| $T_{odt}$ | order-disorder temperature (°C) |
| WSL | weak segregation limit |

## REFERENCES AND NOTES


1. Mizushima, K., Jones, P. C., Wiseman, P. J., Goodenough, J. B. *Mat. Res. Bull*, 1980, **15**, 783–789.
2. Hallinan, D. T., Balsara, N. P. *Annu. Rev. Mater. Res*, 2013, **43**, 503–25.
3. Young, W. S., Kuan, W. F., Epps, T. H. *J. Polym. Sci. Part B Polym. Phys.*, 2014, **52**, 1–16.
4. Morris, M. A., An, H., Lutkenhaus, J. L., Epps, T. H. *ACS Energy Lett.*, 2017, 2, 1919–1936.
5. Soo, P. P., Huang, B., Jang, Y.-I., Chiang, Y.-M., Sadoway, D. R., Mayes, A. M. *J. Electrochem. Soc.*, 1999, **146**, 32–37.
6. Miller, T. F., Wang, Z. G., Coates, G. W., Balsara, N. P. *Acc. Chem. Res.*, 2017, 50, 590–593.
7. Flory, P. J. *J. Chem. Phys.*, 1942, **10**, 51–61.
8. Huggins, M. L. *J. Am. Chem. Soc.*, 1942, **64**, 1712–1719.
9. Leibler, L. *Macromolecules*, 1980, **13**, 1602–1617.
10. de Gennes, P. G. *J. Phys. Lett.*, 1977, **38**, 441–443.
11. de Gennes, P. G. Scaling Concepts in Polymer Chemsitry, Cornell University Press, Ithaca, NY, 1979.
12. Fredrickson, G. H., Liu, a J., Bates, F. S. *Macromolecules*, 1994, **27**, 2503–2511.
13. Helfand, E. *Macromolecules*, 1975, **8**, 552–556.
14. Bates, F. S., Fredrickson, G. H. *Annu. Rev. Phys. Chem.*, 1990, **41**, 525–557.
15. Kawasaki, K., Kawakatsu, T. *Macromolecules*, 1990, **23**, 4006–4019.
16. Cochran, E. W., Garcia-Cervera, C. J., Fredrickson, G. H. *Macromolecules*, 2006, **39**, 2449–2451.
17. Knychała, P., Timachova, K., Banaszak, M., Balsara, N. P. *Macromolecules*, 2017, 50, 3051–3065.
18. Flory, P. J. Principles of Polymer Chemistry, Cornell University Press, Ithaca, 1953.
19. Wang, Z. G. *J. Phys. Chem. B*, 2008, **112**, 16205–16213.

20. Nakamura, I., Wang, Z. G. *Soft Matter*, 2012, **8**, 9356–9367.

21. Ruzette, G., Soo, P. P., Sadoway, D. R., Mayes, A. M. *J. Electrochem. Soc.*, 2001, **148**, A537–A543.

22. Sing, C. E., Zwanikken, J. W., de la Cruz, M. O. *Nat. Mater.*, 2014, **13**, 694–698.

23. Hou, K. J., Qin, J. *Macromolecules*, 2018.

24. Martin, J. M., Li, W., Delaney, K. T., Fredrickson, G. H. *Cit. J. Chem. Phys.*, 2016, **145**, 154104.

25. Ganesan, V., Pyramitsyn, V., Bertoni, C., Shah, M. *ACS Macro Lett.*, 2012, **1**, 513–518.

26. Brown, J. R., Seo, Y., Hall, L. M., Lowrie, W. G. *Phys. Rev. Lett.*, 2018, **120**, 1–7.

27. Armand, M. B. *Annu. Rev. Mater. Sci.*, 1986, **16**, 245–261.

28. Borodin, O., Smith, G. D. *Macromolecules*, 2006, **39**, 1620–1629.

29. Gilbert, J. B., Luo, M., Shelton, C. K., Rubner, M. F., Cohen, R. E., Epps, T. H. *ACS Nano*, 2015, **9**, 512–520.

30. Gartner, T. E., Morris, M. A., Shelton, C. K., Dura, J. A., Epps, T. H. *Macromolecules*, 2018, **51**, 1917–1926.

31. Xie, S., Lodge, T. P. *Macromolecules*, 2018, **51**, 266–274.

32. Teran, A. a., Balsara, N. P. *J. Phys. Chem. B*, 2014, **118**, 4–17.

33. Wanakule, N. S., Virgili, J. M., Teran, A. A., Wang, Z. G., Balsara, N. P. *Macromolecules*, 2010, **43**, 8282–8289.

34. Loo, W. S., Galluzzo, M. D., Li, X., Maslyn, J. A., Oh, H. J., Mongcopa, K. I., Zhu, C., Wang, A. A., Wang, X., Garetz, B. A., Balsara, N. P. *J. Phys. Chem. B*, 2018, **122**, 8065–8074.

35. Gunkel, I., Thurn-Albrecht, T. *Macromolecules*, 2012, **45**, 283–291.

36. Young, W., Epps, T. H. *Macromolecules*, 2009, **42**, 2672–2678.

37. Zardalidis, G., Gatsouli, K., Pispas, S., Mezger, M., Floudas, G. *Macromolecules*, 2015, **48**, 7164–7171.

38. Loo, W. S., Jiang, X., Maslyn, J. A., Oh, H. J., Zhu, C., Downing, K. H., Balsara, N. P. *Soft Matter*, 2018, **14**, 2789–2795.

39. Pesko, D. M., Timachova, K., Bhattacharya, R., Smith, M. C., Villaluenga, I., Newman, J., Balsara, N. P. *J. Electrochem. Soc.*, 2017, **164**, E3569–E3575.

40. Frielinghaus, H., Pedersen, W. B., Larsen, P. S., Almdal, K., Mortensen, K. *Macromolecules*, 2001, **34**, 1096–1104.

41. Zhu, L., Cheng, S. Z. D., Calhoun, B. H., Ge, Q., Quirk, R. P., Thomas, E. L.,

Hsiao, B. S., Yeh, F., Lotz, B. *Polymer (Guildf).*, 2001, **42**, 5829–5839.

42. Nakamura, I. *J. Phys. Chem. B*, 2014, **118**, 5787–5796.

43. Irwin, M. T., Hickey, R. J., Xie, S., Bates, F. S., Lodge, T. P. *Macromolecules*, 2016, **49**, 4839–4849.

44. Maurer, W. W., Bates, F. S., Lodge, T. P., Almdal, K., Mortensen, K., Fredrickson, G. H. *J. Chem. Phys.*, 1998, **108**, 2989–3000.

45. Semenov, A. N. *Macromolecules*, 1993, **26**, 6617–6621.

46. Matsen, M. W., Bates, F. S. *Macromolecules*, 1996, **29**, 1091–1098.

47. Helfand, E., Tagami, Y. *J. Chem. Phys.*, 1972, **56**, 3592–3601.

48. Helfand, E. *J. Chem. Phys.*, 1975, **62**, 1327.

49. Eitouni, H. B., Balsara, N. P. *Phys. Prop. Polym. Handb. 2e*, 2006, 339–356.

50. Matsen, M. W. *Eur. Phys. J. E*, 2010, **33**, 297–306.

51. Uneyama, T., Doi, M. *Macromolecules*, 2005, **38**, 196–205.